

Journal of Mechanics of Materials and Structures

**ENERGY-MAXIMIZING HOLES IN AN ELASTIC PLATE
UNDER REMOTE LOADING**

Shmuel Vigdergauz and Isaac Elishakoff

Volume 14, No. 1

January 2019



ENERGY-MAXIMIZING HOLES IN AN ELASTIC PLATE UNDER REMOTE LOADING

SHMUEL VIGDERGAUZ AND ISAAC ELISHAKOFF

A single hole in an infinite elastic plate is used as the simplest setup to find the hole shape which induces the maximum energy increment in a homogeneous stress field given at infinity. In order to avoid the energy unboundedness trivially caused by jagged shapes with an arbitrarily large number of sharp notches, we restrict our attention to only fully concave shapes with everywhere negative curvature. It goes in parallel with the well-known fact that the energy-minimizing hole shapes are invariably convex. Though rather empirical, this easily verified condition allows us to obtain finite and stable energy maxima at moderate computation cost using the same flexible scheme as in the first author's previous research on optimal shaping of the single energy-minimizing hole. The scheme combines a standard genetic algorithm optimization with an efficient semianalytic direct solver and with an economic shape parametrization, both formulated in complex-variable terms. The results obtained are detailed in tables and graphs. They may stimulate further studies in both theoretical and practical directions.

1. Background and motivation

Thin and flat perforated construction elements are widely employed in engineering design. Fulfilling technological functions, holes weaken the structure and hence may substantially reduce its mechanical performance. This happens due to high stresses and energy local concentration induced by the holes in an applied external field σ^∞ with the components

$$\sigma_{xx}^\infty = P, \quad \sigma_{yy}^\infty = Q, \quad \sigma_{xy}^\infty = 0. \quad (1-1)$$

The resultant stress state of the structure depends on the holes' shapes, areas, and mutual arrangement. Of these geometrical factors, the shapes are less important and less determined. On the one hand, they can be chosen to achieve a more favorable construction stress state which, on the other hand, may be adversely affected by technologically inevitable shape uncertainties, even relatively small ones (in the intuitive sense).

Mathematically, such situations fall either in optimization, i.e., looking for the most favorable solutions, or antioptimization, i.e., searching for the least favorable solutions (with regard to the same certain criterion). Interested readers may consult with [Elishakoff and Ohsaki 2010; Hlaváček et al. 2004; Banichuk and Neittaanmäki 2010]. This paper also adopts the worst-case scenario approach.

Quantitatively, the stress state is assessed by either of two interrelated criteria, each having its own field of application:

Keywords: 2-D elastostatic problem, Kolosov–Muskhelishvili potentials, shape extremization, effective energy, surface roughness, genetic algorithm.

- (A) The stress concentration factor (SCF), that is, the maximum of the von Mises stresses along the hole shapes.
- (B) The energy increment brought by the holes into a given outer stress field. For definiteness purposes, the increment is taken at unit load and normalized by the area of the hole.

Extremization of either (A) or (B) gives some extremal (the “best” or the “worst”) properties of the perforated plate.

The SCF (criterion (A)) is most generally employed when the holes’ shapes are treated deterministically and is found by solving the direct in-plane problem of elastostatics with no optimization involved. One can refer to [Pilkey and Pilkey 2008; Savruk and Kazberuk 2017; Murakami 2017], as well as the review paper [Hardy and Malik 1992].

Shape uncertainties were dealt with probabilistically by Pal’mov [1963] and Sheinin [1972] who developed a probabilistic risk measure. These and other researches were summarized in [Khusu et al. 1975; Vitenberg 1971]. This approach has a drawback which consists in the difficulty of obtaining the needed probabilistic characteristics of the random shapes. Recognizing this difficulty, Givoli and Elishakoff [1992] resorted to an alternative approach where they characterized uncertainty via some integral bounds and correctly exemplified a hypocycloid as the simplest “worst” hole shape. The possible disadvantage of such an approach consists in the possibility that the integral inequality is satisfied and still the shape of the form might possess a very sharp, even if very small, notch with an arbitrarily large SCF. In other words, this criterion, due to its local nature, is unbounded above and so is unsuitable for antioptimization.

At the same time, such a single notch produces only a finite energy increment, even in the limiting case of a needle shape. By this reason, more promising is the stress-averaging energy criterion (B), which can deal with some sort of extremal forms over a wide variety of the holes’ shapes. For examples, the reader may consult [Cherkaev et al. 1998; Vigdergauz 2006; Pedersen et al. 1992; Pedersen 2013]. To the authors’ best knowledge, the only published attempt to analyze the energy-*maximizing* (“worst”) shape was made by Vigdergauz [2006] for the simplest case of a single square symmetric hole in a plate under remote shear by exploiting the semianalytical optimization scheme specially developed for identifying the energy-*minimizing* shapes. As the shape’s design variables, this accepts the first n nonzero terms of the Laurent series of the conformal mapping of the shape sought onto a circle. Expectedly, with increasing n the antioptimized hole shape tends to form a rapidly growing number of small sharp notches (manifested themselves as shape curvature oscillations) whose overall energy increment also grows and actually turns unbounded. By contrast, the energy-*minimizing* process is highly stable even for $n = 4 \div 6$ as shown numerically in [Cherkaev et al. 1998; Vigdergauz 2006].

Remarkably, the resultant optimal holes’ shapes are convex (or, equivalently, have a nonnegative curvature) everywhere, although this was not required *a priori* in the solving procedure. As if reversing the situation, we propose to confine our further antioptimization analysis to only concave shapes with nonpositive curvature and hence avoid generating multiple notches. Computations performed under this restriction show fast convergence (again at $n = 4 \div 6$) to stable finite maxima. These, combined with the previously obtained minimum values, comprise the attainable two-sided bounds on the energy increment for any hole shape of a constant-signed curvature.

Our contribution is therefore three-fold:

- First, the integral-type energy increment is proposed as a new antioptimization criterion instead of the local SCF, which is trivially unbounded in the deterministic (nonprobabilistic) risk maximization.
- Second, the obvious necessity of avoiding the uncontrolled appearance of multiple edge notches is transformed to a rather “natural” and easily verified condition of a nonpositive shape curvature.
- Finally, using the previously developed global optimization scheme, the detailed numerical results are obtained for a single energy-maximizing hole with various degrees p of rotational symmetry under biaxial tension and pure shear. The resultant shapes are close to p -cusped hypocycloids with the energy maximum decreasing at increasing p . Recently, similar curves have been considered by Shahzad et al. [2017] in the related context of out-of-plane elasticity.

The rest of the paper is structured as follows. Section 2 formalizes the problem in terms of the relevant analytical background. Section 3 details the proposed three-component algorithm which provides a stable numerical solution of the antioptimization problem at hand. The results obtained are presented and discussed in Section 4. Our findings are summarized in Section 5. Some new analytical derivations are placed in the Appendix.

2. Proposed model and basic equations

Locate an isotropic and linearly elastic infinite plate in the plane of a complex variable $z = x + iy$. Let the plate contain a single traction-free hole with a piecewise smooth boundary L enclosing the origin of the Cartesian system xOy . Let also the contour L be composed of p convex or concave identical smooth arcs λ_j , $j = \overline{1, p}$ sequentially rotated around the origin. They form p connection points, possibly irregular, as exemplified in Figure 1 for $p = 4$. In what follows, we denote these shapes as L_p , $p = 2, 3, \dots$, retaining the notation L for general closed curves. The assumption of the constant-signed arcs' curvature will be shown to be crucial for the optimization analysis performed in the next sections.

To facilitate further general derivations, we parameterize a shape L with a real angular variable θ along the unit circle γ :

$$L : t = \omega(\xi), \quad \xi = \exp i\theta \in \gamma, \quad \bar{\xi} = \xi^{-1}, \quad |\xi| = 1, \quad (2-1)$$

where $\omega(\zeta)$ is the univalent analytic function informally mapping the exterior $\Sigma : |\zeta| \geq 1$ of γ onto the considered elastic domain S :

$$\Sigma + \gamma \xrightarrow[\omega(\zeta)]{} S + L, \quad \omega(\zeta) = \zeta + \sum_{k=1}^{\infty} d_k \zeta^{-k}. \quad (2-2)$$

Without loss of generality, say L is placed symmetrically with respect to the x -axis and, hence, the coefficients $\{d_k\}$ are pure real.

The traction-free condition along the hole boundary reads

$$\sigma_{\rho\rho}(t), \sigma_{\rho\tau}(t) \equiv 0, \quad t \in L, \quad (2-3)$$

where $\sigma(t) = \{\sigma_{\rho\rho}, \sigma_{\tau\tau}, \sigma_{\rho\tau}\}$ stands for the stress tensor in a local system of curvilinear orthogonal coordinates (ρ, τ) at a point $t \in L$.

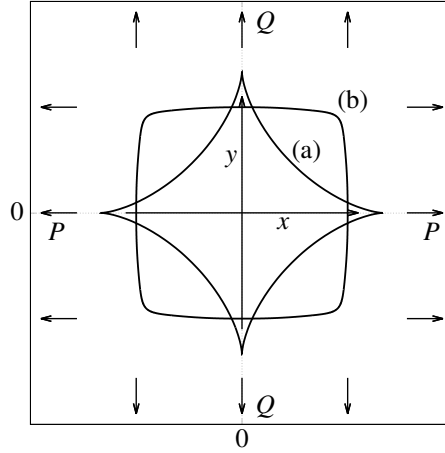


Figure 1. The problem schematic: an infinite plate with a traction-free hole under uniform stresses. The cases $P = Q$ and $P = -Q$ correspond to remote bulk and shear, respectively. The piecewise smooth hole boundary possesses a certain rotational symmetry and is either concave (a) or convex (b) everywhere except possibly at a finite number of angular points.

Under a given remote load (1-1), the plate is in plain strain or plain stress, so displacements or gradients in the out-of-plane direction may be omitted from consideration. Then the resultant state of stress in the auxiliary domain $\Sigma + \gamma$ can be effectively described by a pair of the Kolosov–Muskhelishvili (KM) potentials [Muskhelishvili 1963], which are complex-valued analytic functions in Σ and continuously extendible to γ , with far-field asymptotics (1-1):

$$\Phi_0(\zeta) = B + \Phi(\zeta), \quad \Psi_0(\zeta) = \Gamma + \Psi(\zeta), \quad \zeta \in \Sigma, \quad \Phi(\zeta), \Psi(\zeta) = O(|\zeta|^{-2}); \quad (2-4a)$$

$$4B = \text{Tr}\{\sigma^\infty\} = Q + P, \quad 2\Gamma = \text{Dev}\{\sigma^\infty\} = Q - P, \quad \text{Im } B, \text{Im } \Gamma = 0, \quad (2-4b)$$

and convergent series expansions

$$\Phi(\zeta) = \sum_{k=2}^{\infty} a_k \zeta^{-k}, \quad \Psi(\zeta) = \sum_{k=2}^{\infty} b_k \zeta^{-k}, \quad \zeta \in \Sigma + \gamma. \quad (2-5)$$

The local stresses are related to $\Phi_0(\zeta)$, $\Psi_0(\zeta)$ through the commonly known formulae which are not displayed here to save room. The first order items $\sim \zeta^{-1}$ must be zero to match the static state conditions [Muskhelishvili 1963].

Substituting (2-4a) into (2-3) yields the boundary condition for the KM potentials $\Phi(\zeta)$, $\Psi(\zeta)$ vanishing at infinity:

$$-\frac{2}{\xi^2} \overline{\omega'(\xi)} [\text{Re } \Phi_0(\xi) + B] + \overline{\omega(\xi)} \Phi_0'(\xi) + \Gamma \omega'(\xi) = -\omega'(\xi) \Psi_0(\xi), \quad \xi \in l. \quad (2-6)$$

The terms in (2-6) are rearranged specifically for later use.

By integrating (2-6) over γ , one gets the hole-induced energy increment δW as a linear combination of the leading coefficients a_2, b_2 (see, for instance, [Vigdergauz 2001]):

$$\delta W = 2\pi f^{-1}(2\Gamma a_2 + B b_2), \quad (2-7)$$

where f signifies the hole area, by which δW is normalized.

For dimensional reasons, a_2, b_2 are proportional to f [Muskhelishvili 1963]:

$$a_2 = \alpha_2 f, \quad b_2 = \beta_2 f, \quad (2-8)$$

and hence, equivalently,

$$\delta W = 2\pi(2\Gamma\alpha_2 + B\beta_2). \quad (2-9)$$

So, in fact, (2-7) and (2-9) present the energy density that is the hole-induced energy stored in the plate and taken per hole area unit. At given remote loading this quantity depends only on the hole shape. In particular, for a circle ($t \in L, |t|^2 = R^2, \omega(\xi) = \xi$), one has [Muskhelishvili 1963]

$$\Phi(\xi) = \frac{\Gamma R^2}{\xi^2}, \quad \Psi(\xi) = \frac{2BR^2}{\xi^2} + 3\frac{\Gamma R^4}{\xi^4}, \quad \alpha_2 = \frac{\Gamma}{\pi}, \quad \beta_2 = \frac{2B}{\pi}, \quad (2-10)$$

and therefore,

$$\delta W = 4(\Gamma^2 + B^2). \quad (2-11)$$

By the residues theorem [Ahlfors 1953], the hole area f is expressed in current terms as

$$f = \frac{1}{2i} \int_L \bar{t} dt = \frac{1}{2i} \int_\gamma \overline{\omega(\xi)} \omega'(\xi) d\xi = \pi \left(1 - \sum_{k=1}^{\infty} k |d_k|^2 \right). \quad (2-12)$$

Similarly, some other useful integrals are (where $\delta_{n,0}$ is the Kronecker delta)

$$\frac{1}{2\pi i} \int_L t^n dt = 0, \quad \frac{1}{2\pi i} \int_L \frac{dt}{t^n} = \delta_{n,1}, \quad n = 0, 1, \dots, \quad t \in L, \quad (2-13)$$

and [Muskhelishvili 1963]

$$2\pi i B + 2Im \int_\gamma \overline{\phi(\xi)} \omega'(\xi) d\xi = - \int_\gamma \psi(\xi) \omega'(\xi) d\xi = 2\pi i b_2, \quad (2-14)$$

where

$$\phi'(\xi) = \omega'(\xi) \Phi(\xi), \quad \psi'(\xi) = \omega'(\xi) \Psi(\xi). \quad (2-15)$$

3. Problem formulation and solution scheme

We are now in a position to quantitatively rephrase the 2-D shape antioptimization problem at hand in complex-variable terms.

Given a far stress field (B, Γ) find a p -cusped hole boundary L_p which maximizes the normalized increment (2-9):

$$\delta W(B, \Gamma, L_p) \xrightarrow{\{L_p\}} \max(B, \Gamma, p). \quad (3-1)$$

Recall that L_p is defined in Section 1 as composed of p identical arcs with constant-signed curvature κ . Pure geometrical considerations give [Pólya and Szegő 1972, part 3, problem 108]

$$\kappa(t) \equiv \frac{1}{\rho(t)} = \frac{1 + \operatorname{Re}(\tau \omega''(\tau)/\omega'(\tau))}{|\tau \omega'(\tau)|}, \quad t = \omega(\tau) \in L, \quad \tau \in \gamma, \quad (3-2)$$

where $\rho(t)$ is the radius of curvature (reciprocal of curvature) at a point $t \in L$.

Since the denominator in the right-hand side of (3-2) is always nonnegative, the hole boundary is non-convex (nonconcave) everywhere if and only if the numerator is nonpositive (nonnegative), respectively, along the basic arc λ_1 :

$$\operatorname{Re}\left(\tau \frac{\omega''(\tau)}{\omega'(\tau)}\right) \xrightarrow{\forall \tau \in \lambda_1} \begin{cases} \text{concave if } \leq -1, \\ \text{convex if } \geq -1. \end{cases} \quad (3-3)$$

This easily verified condition effectively restricts the optimization process to target only the L_p -type shapes as required.

In general, (3-1) cannot be performed analytically, except in some simple but nontrivial cases described below, though numerically this is a rather standard problem. Its solution is conveniently obtained by an iterative loop over successively modified shapes while computing the criterion (fitness function) of each feasible candidate selected from the predefined pool $\{L_p\}$. For this purpose, a specially tailored approach was developed and validated in the first author's previous papers (see, for instance, [Vigdergauz 2006]). It includes three main ingredients:

- an efficient and adaptive shape parametrization scheme,
- an enhanced direct solver to evaluate the energy increment for an arbitrarily given shape, and
- a genetic algorithm (GA) approach as the antioptimum search engine.

Their peculiarities are briefly outlined in the next subsections for reader's convenience.

3.1. Shape parametrization scheme. For numerical purposes, the infinite Laurent expansion (2-2) is commonly truncated to the first M terms. In the current context, it is justified *a posteriori* by the fact that with increasing M the GA approximations do converge rapidly to a stable solution under the restriction (3-3). Geometrically, higher coefficients in (2-2) are responsible for quickly changing local elements of the mapped shape which inevitably violate the constant signed curvature requirement. Otherwise, the antioptimized shape tends to form acute-angled cusps and teeth resulting in unbounded growth of the energy increment as compared at the top right of Figure 4 in Section 4.

Independently of (3-3), coefficients $\{d_j\}$ must fall into the successfully narrowing intervals

$$-1/\sqrt{k} \leq d_k \leq 1/\sqrt{k}, \quad k = 1, 2, \dots \quad (3-4)$$

to provide one-to-one mapping between L and γ [Ahlfors 1953]. This allows us to treat these intervals as linear constraints in the maximization problem (3-1) and hence encode the pool $\{L_p\}$ of shapes through an ordered M -length string of real numbers $(b_k, k = \overline{1, M})$ which form an M -dimensional hyper-rectangle Π_M where any shape is presented with a point specified by its coordinates. This scheme is used to perform numerical single-objective global maximization of the energy increment over a wide range of design variables $\{d_k\}$ subject to the nonstrict inequality constraint (3-3).

Remark. Inequalities (3-4) are necessary, but are on no account sufficient conditions for the mapping uniqueness. However, in numerical practice it is desirable to accelerate the computations by narrowing these intervals. To our best knowledge, it can be done only for the one-term mapping

$$\omega(\xi) = \xi + d_k/\xi^k, \quad |d_k| \leq 1/k, \quad k \geq 1, \quad (3-5)$$

where the right inequality is necessary and sufficient to prevent self-crossing of L . However, simple geometrical arguments show that for any shape the constant-signed curvature (3-3) is a more restrictive requirement than the mapping uniqueness which, therefore, has no need to be checked separately. The case of an ellipse ($k = 1$) is excluded as impractical for the current problem since its limiting one-to-one map degenerates in a straight slit with zero area $f = 0$. Otherwise this limit corresponds to a p -cusped hypocycloid ($k = p - 1$, $d_k = \pm(p - 1)$) with $f = 1 - 1/(p - 1)$ and the negative curvature

$$\kappa(\theta) = -\frac{p-2}{4} \csc\left(\frac{1}{2}p\theta\right), \quad 0 \leq \theta \leq 2\pi, \quad p = 3, 4, \dots \quad (3-6)$$

Here and henceforth, the opposite signs in d_k indicate rotation through the angle π/p .

In the next subsection this L_p shape is proven to solve the antioptimization problem with only one of the two orientations corresponding to the global energy maximum.

3.2. Direct solver. Equation (2-6) states that its left side is the boundary value of a function holomorphic outside the unit circle γ and vanishing at infinity, which thus has no nonnegative powers of ζ as actually taken in the Laurent series (2-5) for $\Psi(\xi)$. However, substitution of the first expansion from (2-5) and (2-2) into (2-6) does produce these powers with the coefficients composed of a_k , d_k , and integers. The reason is the conjugation operation over ζ : $\bar{\zeta}^k = \xi^{-k}$, $k = \pm 1, \pm 2, \dots$. By equating them to zero, Kalandiya [1975] gets an infinite system of linear algebraic equations in the unknowns $\{a_k\}$ only:

$$a_{m+2} - \sum_{k=1}^m (m-k+1) \bar{d}_{m-k+1} a_k - (m+1) \sum_{k=1}^{\infty} \bar{d}_{m+k+1} \bar{a}_k = A_m, \quad m = 0, 1, \dots; \quad (3-7a)$$

$$A_0 = 2B - \Gamma, \quad A_1 = 0, \quad A_m = -2B(m+1) \bar{d}_{m+1}, \quad m \geq 2, \quad (3-7b)$$

with no coefficients of $\Psi(\xi)$. These can be simply restored afterwards through (2-6) and (2-13), when needed. The first sum in (3-7a) is omitted for $m = 0, 1$.

Remarkably, for any M -term finite mapping ($d_k = 0$, $\forall k > M$), the system (3-7) also shrinks to the first M equations in the unknowns a_k , $k = 1, \overline{M}$ while the infinite remainder of them in the unknowns a_k , $k > M$ is next solved analytically by a finite differences technique [Vigdergauz 2006].

As applied to $\omega(\zeta)$, the p -fold symmetry states that only d_{pl-1} , $l = 1, 2, \dots$, differ from zero so that $M = np - 1$, where n is a new truncation parameter which also governs the solution, though in a different way. While M appears implicitly in the resolving system (3-7), n serves as the number of design variables in the optimization encoding/decoding scheme (see the next subsection).

For better clarity, two basic loadings of different rotational symmetry and analytical peculiarities are considered separately, those of square-antisymmetric pure shear ($B = 0$, $\Gamma = 1$) and isotropic bulk loading ($2B = 1$, $\Gamma = 0$). In either case, the coefficients $\{a_k\}$ could also partially vanish due to adopted p -fold symmetry of the hole shape, thus further diminishing the system size from M to $N < M$ in nonzero unknowns a_k , $k = 1, 2, \dots, N$.

3.2.1. Pure shear. Here the coefficient β_2 disappears in the energy increment expression $\delta W = 4\alpha\Gamma^2$, which can be obtained by taking directly from the solution of the $(N \times N)$ truncated system (3-7). This case has been studied in detail previously [Vigdergauz 2006] though the energy maxima were not considered there. Particularly, for only one nonzero mapping term ($n = 1$) we have:

- A triangular symmetry ($p = 3, M = 2, N = 1$):

$$a_2 = 1, \quad \delta W_2 = \frac{4}{(1 - 2d_2^2)}, \quad \min_{d_2} \delta W_2 = \delta W_2^{(\min)} = 4, \quad d_2^{(\min)} = 0, \quad (3-8a)$$

$$\max_{d_2} \delta W_2 = \delta W_2^{(\max)} = 8, \quad d_2^{(\max)} = \pm \frac{1}{2}. \quad (3-8b)$$

- A square symmetry ($p = 4, M = 3, N = 1$):

$$a_2 = \frac{1}{1 - d_3}, \quad \delta W_3 = \frac{4}{(1 - d_3)(1 - 3d_3^2)} \quad (3-9a)$$

$$\delta W_3^{(\min)} = \frac{9}{\sqrt{2} + 1}, \quad d_3^{(\min)} = \frac{1 - \sqrt{2}}{3}, \quad (3-9b)$$

$$\delta W_3^{(\max)} = 9, \quad d_3^{(\max)} = \frac{1}{3}. \quad (3-9c)$$

- A more-fold symmetry ($p \geq 5, M = p - 1, N = 2$):

$$a_2 = \frac{1}{1 - (M - 1)d_M^2}, \quad \delta W_p = \frac{4}{(1 - (M - 1)d_M^2)(1 - Md_M^2)}, \quad (3-10a)$$

$$\delta W_p^{(\min)} = 4, \quad d_M^{(\min)} = 0, \quad (3-10b)$$

$$\delta W_p^{(\max)} = \frac{4M^3}{(M^2 - M + 2)(M - 1)}, \quad d_M^{(\max)} = \pm \frac{1}{M}. \quad (3-10c)$$

We note that only the case $p = 4$ is sensitive to the hypocycloid angular position as given by the sign of d_3 . It produces the global energy maximum (3-9c) when aligned with the main stresses directions ($d_3 = \frac{1}{3}$) and the halved value $\delta W = 4.5$ otherwise.

3.2.2. Bulk loading. With solved $a_k, k = \overline{1, M}$, the Ψ -related coefficient b_2 is arrived at analytically by a little algebra as detailed in the Appendix. Again, as before, the case $n = 1$ takes a simple closed form ($M = p - 1$):

$$\delta W(d_M) = 4B^2 \frac{1 + Md_M^2}{1 - Md_M^2}, \quad \delta W_M^{(\max)} = \frac{4(M+1)}{M-1}, \quad d_M^{(\max)} = \pm \frac{1}{M}. \quad (3-11)$$

The above formulas suggest two analytical conclusions for $n = 1$:

- (A) for any $p > 2$ and either loading the energy-maximizing hole shape with constant-signed curvature is an everywhere concave p -cusped hypocycloid, or
- (B) the associated energy maximum monotonically decreases with increasing p .

In the general case of $n > 1$ these are numerically extended in the next section.

The subsection is concluded with the following summarizing observation. It is a matter of direct verification to prove that a hypocycloid is the only fully concave one-term mapping (3-5). All smaller

values of $|d_k|$ give raise to convex zones gradually expanding from the vertices. Put it differently, under the concavity requirement, the searching space $\{L_p\}$ is nontrivially populated only for $n > 1$

3.3. The global optimization scheme. The design variables $(a_k, k = \overline{1, M})$ must meet the constant-signed curvature condition (3-3), otherwise they are free to vary in large intervals (3-4). Due to the nature of the objective function δW , the maximization problem (3-1) may have many local maxima even though the number M of design variables is small (at most six in our numerical simulations). This circumstance precludes the use of exhaustive search or traditional descent methods.

An effective alternative is provided by an evolutionary-type genetic algorithm (GA). Devised by Holland [1975], it has become well-accepted in the last several decades (see, for instance, [Goldberg and Sastry 2007]). This heuristic approach performs a gradientless optimization in a large search space by mimicking the Darwinian process of natural selection over successive generations through blind crossover and mutation operations. The major advantage of the GA is that it explores the solution space by testing parameter combinations simultaneously to avoid local extrema of the objective function, and requires no derivative information [Goldberg and Sastry 2007].

The GA operates by constructing a population of M -strings and finds δW for each string. These are encoded using a discrete 16-bit procedure where each design variable is represented only by $2^{16} - 1$ separate values in the continuous search space. In view of (3-4), this representation is decoded from a randomly generated integer (or gene) $v \in [-I; I]$, $I = 2^{15}$ as $d_k = v/I\sqrt{k}$, $k = \overline{1, M}$. The genes for different coefficients are concatenated into an ordered $16N$ binary set, or chromosome, that encodes a set of design variables. The chromosome's fitness value is obtained by solving the corresponding direct problem of finding δW while checking the restriction (3-3) at 100 points equally spaced in the irreducible interval $\theta \in [0; \pi/p]$. Once a randomly generated set's population has been evaluated, bitwise crossover and mutations are next applied to the chromosomes with a certain probability level, thus producing the next generation. Then the process is successively repeated to gradually increase the species' fitness δW in the long run. In view of this, wherever (3-3) is violated, the corresponding set obtains a penalty as its fitness, and the GA process takes the next candidate. The idea is to make the set noncompetitive by assigning the penalty, as the squared violation is multiplied by a very large negative constant. The optimization is stopped after some N_{iter} iterations — in belief that the process really converges. Practically, N_{iter} is chosen in such a way that the optimization criterion remains unchanged in successive iterations well in advance of termination.

For the reader's convenience, Table 1 summarizes the above-introduced governing parameters.

After adjusting the heuristic probability levels of the GA operations, this scheme was used to obtain the numerical results presented in the next section. In order to prevent the GA process against possibly being “stuck” quite far from the global maximum, multiple runs are carried out in the current work for each separate problem at the given number n of nonzero mapping terms. Motivated by the proposed optimization strategy, we form a sequence of approximations in ascending order of n , which converges rapidly to a stable hole shape.

4. Numerical results

4.1. Pure shear ($Q = -P : B = 0, \Gamma = 1$). For illustration purposes, the number p of the contour cusps is chosen here as a power of two to better match the square antisymmetry of loading.

GA parameter	parameter value(s)
gene	integer $[-2^{31}; 2^{31}]$
individual	interface shape
degree of the shape's rotational symmetry (p)	integer $3 \div 128$
population size	$20000 \div 50000$ (depending on the parameter p)
number of genes (n)	up to 6
number of nonzero mapping terms	depending on parameter p
truncation size of the conformal mapping (M)	$pn - 1$
resolving system size (N)	$\leq M$
initial population	$20000 \div 50000$ random individuals
selection	tournament
elitism	four best individuals
crossover	1-point
crossover rate	0.99
creep mutation	by randomly changing a bit
creep mutation rate	0.35
jump mutation	by adding a random integer value typically $[-2^9; 2^9]$
jump mutation rate	0.35
stopping criterion (N_{iter})	after $100 \div 150$ iterations

Table 1. GA operator types, their probability rates, and related parameters typically used in further optimizations.

n	M	d_3	d_7	d_{11}	d_{15}	d_{19}	d_{23}	$\delta W_4^{(\max)}$
1	3	0.33333						9.000
2	7	0.39461	-0.02626					11.967
3	11	0.43363	-0.05303	0.00648				15.613
4	15	0.43504	-0.06192	0.01431	-0.00194			16.069
5	19	0.43644	-0.06037	0.01212	-0.00164	0.00024		16.172
6	23	0.43785	-0.05794	0.01009	-0.00164	0.00024	$4.45 \cdot 10^{-5}$	16.259

Table 2. Pure shear. A single square symmetric ($p = 4$) hole: the antioptimal mapping coefficients and the global criterion $\delta W_4^{(\max)}$ for different values of n and $M = 4n - 1$.

Table 2 confirms the expected fast convergence of the GA approximations to the steady state solution after the few first values of n , which is typical for any p . Figure 3 shows the evolution of the antioptimal holes from the single ($n = 1$) to multiterm stable ($n = 4 \div 6$) shape.

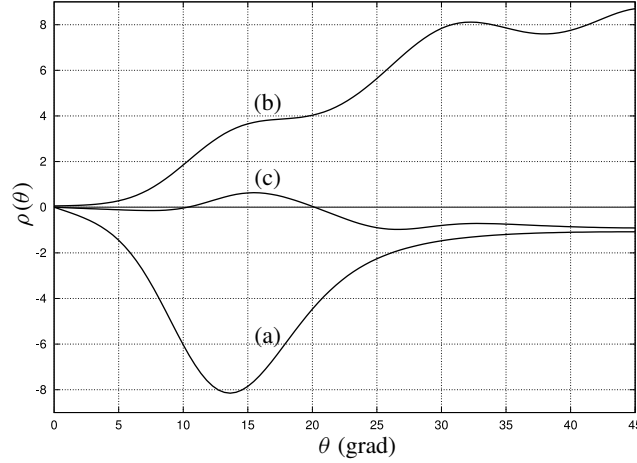


Figure 2. Pure shear. The curvature radii $\rho(\theta)$ for the energy-extremal holes with square symmetry ($p = 4$).

p	$\delta W_p^{(\max)}$	$\delta W_p^{(\min)}$	$\delta W_p^{(\max)}/\delta W_p^{(\min)}$
4	16.259	3.71449	4.377
8	6.975	4.0	1.744
16	5.289	4.0	1.322
32	4.571	4.0	1.143
64	4.141	4.0	1.035
128	4.067	4.0	1.017

Table 3. Pure shear. The energy extrema attained at the maximizing and minimizing hole shapes with different degrees p of rotational symmetry and constant-signed curvature. The value $\delta W_p^{(\min)}$ at $p = 4$ is obtained by GA optimization in [Vigdergauz 2006].

Table 3 displays the stable values of $\delta W_p^{(\max)}$ and $\delta W_p^{(\min)}$ numerically computed at $n = 4 \div 6$ for shapes of constant negative and constant positive curvature, respectively. The allowed energy interval $\Delta W_p \equiv [\delta W_p^{(\min)}; \delta W_p^{(\max)}]$ is seen to shrink gradually to the point $\delta W_p^{(\max)} = \delta W_p^{(\min)} = 4$ with increasing p and

$$\max_p \Delta W_p^{(\text{shear})} = \Delta W_4^{(\text{shear})} = [3.714; 16.259]; \quad \lim_{p \rightarrow \infty} \Delta W_p^{(\text{shear})} \rightarrow [4; 4]. \quad (4-1)$$

The subsection is concluded with Figure 2 outlining how the signed curvatures radii $\rho(\theta)$ of different extremal shapes (indicated in the previous figure by the same letters) relate to each other. For easier comparison, the energy minimizing shape (b) is first rotated through 45° to be oriented like the two others. In the absence of restriction (3-3), the resultant shape (c) is seen to form zones of high curvature with alternating sign located near the vertices and is associated with unlimited growth of the energy increment [Vigdergauz 2006].

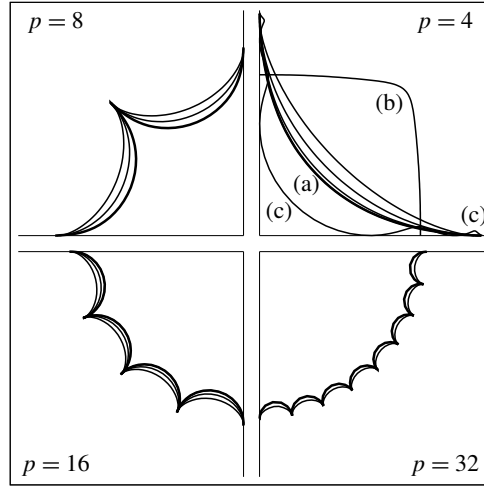


Figure 3. Pure shear. Evolution of the energy-maximizing p -cusped concave hole shapes with increasing number N of the conformal mapping terms to the limiting (boldfaced) curves. The energy-minimizing (b) and the extremal cross-like (c) contours [Vigdergauz 2006] at $n = 23$ are also added for contrast.

n	M	d_2	d_5	d_8	d_{11}	d_{14}	$\delta W_3^{(\max)}$
1	2	0.5					3.000
2	5	0.55786	-0.02315				4.188
3	8	0.60657	-0.05161	0.00561			6.448
4	11	0.61837	-0.06120	0.00988	-0.00089		7.616
5	14	0.62062	-0.06233	0.01026	-0.00112	$4.89E-05$	7.753

Table 4. Bulk loading. A single symmetric triangular ($p = 3$) hole: the antioptimal mapping coefficients and the global criterion $\delta W_3^{(\max)}$ for different values of n and $M = 3n - 1$.

4.2. Bulk loading ($Q = P : 2B = 1, \Gamma = 0$). Since this load is isotropic, the problem's rotational symmetry is determined only by parameter p , which is chosen here as a multiple of 3.

The results are organized like in the previous subsection. Table 4 exemplifies the GA convergence process for $p = 3$. Figure 4 presents the L_p shape's evolution to the steady state form with increasing parameter n .

Other computational findings (not displayed here to save space but available from the authors) indicate that with increasing p the stable values of $\delta W_p^{(\max)}$ expectedly decrease to the commonly known p -independent global minimum $W_p^{(\min)} = 4$ invariably achieved at a circle. Here,

$$\max_p \Delta W_p^{(\text{bulk})} = \Delta W_3^{(\text{bulk})} = [1; 7.753]; \quad \lim_{p \rightarrow \infty} \Delta W_p^{(\text{bulk})} \rightarrow [1; 1]. \quad (4-2)$$

A close inspection of Tables 2 and 4 suggests the following general observations, providing a deeper understanding of how the proposed maximization criterion (2-9) works:

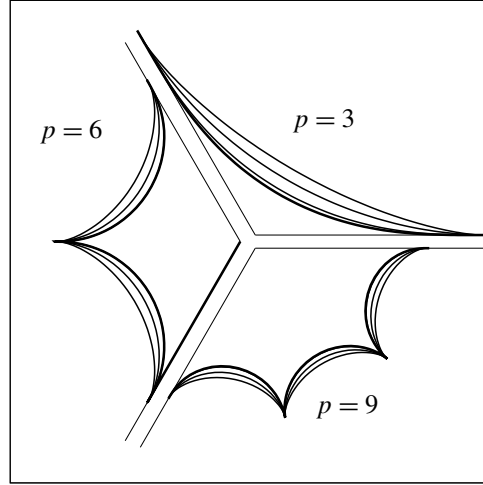


Figure 4. The bulk loading case. Evolution of the energy-maximizing p -cusped concave hole shapes with increasing number N of the conformal mapping terms to the limiting (boldfaced) curves.

- At given n , each table row forms a sequence of rapidly vanishing mapping coefficients. It seems like each next coefficient tends to correct the previous one with aim to increase the shape-induced energy while preserving the arc concavity. Then the coefficients' alternative signs implicitly indicate a good numerical stability of the antioptimization process.
- The resultant leading coefficient d_{p-1} lies outside the empirical interval (3-5) — though, of course, within the wider necessity bounds (3-4):

$$\frac{1}{p-1} \leq |d_{p-1}| \leq \frac{1}{\sqrt{p-1}}, \quad p = 3, 4, \dots \quad (4-3)$$

With increasing p , this interval monotonously shrinks to the zero-point, thus giving no room for antioptimization under the imposed concavity assumption. That is just the reason why with growing p , the energy maximum also shrinks to the limiting value attained at zero mapping coefficients $\{d_k\}$ (a circular hole).

A separate remark is necessary about the case ($p = 4$). For both loadings, the GA-obtained energy *maximizing* shapes (shown in upper right of Figure 3) are practically the same (if not identical), unlike the energy-*minimizing* ones which differ markedly from each other.

5. Conclusions

In concluding we summarize the basic assumptions under which the considered optimization problem has been effectively solved by the simplest GA scheme combined with the semianalytical direct solver:

- The chosen energy increment is the antioptimization criterion of an averaging rather than local nature. It allows the avoidance of the “epsilon technique” used, say, in [Givoli and Elishakoff 1992; Pal'mov 1963] for upper prebounding the hoop stresses.

- Instead, the global nonparametric restriction of constant-signed curvature is imposed to form a practically representative searching pool of the energy-maximizing holes' shapes with a finite increment. This restriction is easily verified numerically by conformal mapping technique within the simple, robust, and computationally efficient direct solver.

As a result it turns out that the energy increments possess a high but stable sensitivity to random disturbances of the fully concave/convex hole shapes, and hence can be accurately evaluated with moderate computing effort.

The results numerically obtained here complement those for the energy-*minimizing* shapes in [Vigdergauz 2006]. Taken together, they provide new two-sided bounds on the hole-induced energy increment, which are exact within the constant-signed curvature constraint. Their widest gaps over parameter p for the basic load cases are given in (4-1) and (4-2).

Appendix: An analytical solution of the master system (3-7) for remote bulk load

Though the unknowns a_k , $k > M$ are outside the scope of the energy increment expression (2-7), they are needed to restore the first KM potential, and hence to evaluate the boundary hoop stresses [Muskhelishvili 1963]

$$\sigma_{\theta\theta}(\xi) = 4 \operatorname{Re} \Phi_0(\xi) = 4B + 4 \sum_{k=2}^{\infty} a_k \cos(k\theta), \quad \xi \in L. \quad (\text{A-1})$$

For pure shear ($B = 0 \rightarrow A_m = 0, \forall m > 2$) the above Fourier series can also be summed up analytically [Vigdergauz 2006] by applying the standard finite differences technique [Levi and Lessman 1992] to the infinite homogeneous system with the load-independent constant coefficients $1, 0, -d_1, -2d_2, \dots, -Md_M$ of the actual bandwidth n resulted from (3-7) for $m > M - 1$ when the second sum apparently disappears:

$$a_{m+2} - \sum_{k=1}^M k d_k a_{m-k+1} = 0, \quad m = M, M+1, \dots \quad (\text{A-2})$$

$\Phi_0(\xi)$ is then expressed as

$$\Phi_0(\xi) = \frac{R_M(\bar{\xi})}{\xi \omega'(\xi)}, \quad (\text{A-3})$$

where $R_M(\xi)$ is a polynomial of degree M in ξ , given as

$$R_M(\xi) = r_M \xi^M + r_{M-1} \xi^{M-1} + \dots + r_0, \quad (\text{A-4})$$

with the coefficients

$$r_0 = a_1 = 0, \quad r_1 = a_2, \quad r_m = a_{m+1} - \sum_{k=2}^m (-1)^k (k) d_k a_{m+k+1}, \quad m \geq 2, \quad (\text{A-5})$$

which may partially vanish owing to the rotational symmetry.

Remarkably, the solution (A-3) is valid also for the bulk loading case corresponding to the same homogeneous ($D_m = 0, \rightarrow A_m = 0, m = M, m = M+1, \dots$) system (A-2). Then, from (2-15) it follows

that

$$\phi'(\xi) = \frac{R_n(\bar{\xi})}{\xi} = \sum_{m=1}^M \frac{r_m}{\xi^{m+1}}; \quad \phi(\xi) = - \sum_{m=1}^M \frac{r_m}{m\xi^m}. \quad (\text{A-6})$$

Finally, substitution of (A-6) into (2-15) gives, while making use of (2-13),

$$b_2 = 2 \left(B + \sum_{m=1}^M d_m r_m \right). \quad (\text{A-7})$$

Particularly, for $n = 1$ the above expressions are simplified to

$$r_M = B M d_M, \quad b_2 = 2B(1 + M d_M^2), \quad \beta_2 = \frac{b_2}{f} = 2B \frac{1 + M d_M^2}{\pi(1 - M d_M^2)}, \quad (\text{A-8})$$

thus arriving at (3-11).

References

- [Ahlfors 1953] L. V. Ahlfors, *Complex analysis*, McGraw-Hill, New York, 1953.
- [Banichuk and Neittaanmäki 2010] N. V. Banichuk and P. J. Neittaanmäki, *Structural optimization with uncertainties*, Solid Mech. Appl. **162**, Springer, 2010.
- [Cherkaev et al. 1998] A. V. Cherkaev, Y. Grabovsky, A. B. Movchan, and S. K. Serkov, “The cavity of the optimal shape under the shear stresses”, *Int. J. Solids Struct.* **35**:33 (1998), 4391–4410.
- [Elishakoff and Ohsaki 2010] I. Elishakoff and M. Ohsaki, *Optimization and anti-optimization of structures under uncertainty*, Imperial College Press, London, 2010.
- [Givoli and Elishakoff 1992] D. Givoli and I. Elishakoff, “Stress concentration at a nearly circular hole with uncertain irregularities”, *J. Appl. Mech. (ASME)* **59**:2S (1992), S65–S71.
- [Goldberg and Sastry 2007] D. E. Goldberg and K. Sastry, *Genetic algorithms: the design of innovation*, 2nd ed., Springer, 2007.
- [Hardy and Malik 1992] S. J. Hardy and N. H. Malik, “A survey of post-Peterson stress concentration factor data”, *Int. J. Fatigue* **14**:3 (1992), 147–153.
- [Hlaváček et al. 2004] I. Hlaváček, J. Chleboun, and I. Babuška, *Uncertain input data problems and the worst scenario method*, North-Holland Series Appl. Math. Mech. **46**, Elsevier, Amsterdam, 2004.
- [Holland 1975] J. H. Holland, *Adaptation in natural and artificial systems*, Univ. Michigan Press, Ann Arbor, 1975.
- [Kalandiya 1975] A. I. Kalandiya, *Mathematical methods of two-dimensional elasticity*, Mir, Moscow, 1975.
- [Khusu et al. 1975] A. P. Khusu, Y. R. Vitenberg, and V. A. Pal'mov, *Шероховатость поверхностей*, Izdat. “Nauka”, Moscow, 1975.
- [Levi and Lessman 1992] H. Levi and F. Lessman, *Finite difference equations*, Dover, New York, 1992.
- [Murakami 2017] Y. Murakami, *Theory of elasticity and stress concentration*, Wiley, Chichester, 2017.
- [Muskhelishvili 1963] N. I. Muskhelishvili, *Some basic problems of the mathematical theory of elasticity*, Noordhoff, Groningen, 1963.
- [Pal'mov 1963] V. A. Pal'mov, “State of stress in the neighborhood of a rough surface of elastic bodies”, *Prikl. Mat. Mekh.* **27**:5 (1963), 963–969. In Russian; translated in *J. Appl. Math. Mech.* **27**:5 (1963), 1479–1489.
- [Pedersen 2013] N. L. Pedersen, “Optimization of bolt thread stress concentrations”, *Arch. Appl. Mech.* **83**:1 (2013), 1–14.
- [Pedersen et al. 1992] P. Pedersen, L. Tobiesen, and S. H. Jensen, “Shapes of orthotropic plates for minimum energy concentration”, *J. Struct. Mech.* **20**:4 (1992), 499–514.

- [Pilkey and Pilkey 2008] W. D. Pilkey and D. F. Pilkey, *Peterson's stress concentration factors*, 3rd ed., Wiley, New York, 2008.
- [Pólya and Szegő 1972] G. Pólya and G. Szegő, *Problems and theorems in analysis, I: Series, integral calculus, theory of functions*, Grundlehren der Math. Wissenschaften **193**, Springer, 1972.
- [Savruk and Kazberuk 2017] M. P. Savruk and A. Kazberuk, *Stress concentration at notches*, Springer, 2017.
- [Shahzad et al. 2017] S. Shahzad, F. Dal Corso, and D. Bigoni, “Hypocycloidal inclusions in nonuniform out-of-plane elasticity: stress singularity vs. stress reduction”, *J. Elasticity* **126**:2 (2017), 215–229.
- [Sheinin 1972] V. I. Sheinin, “On asymptotic method of calculation of stresses near the rough surface of elastic bodies”, *Izv. Akad. Nauk SSSR Mekh. Tverd. Tela* **2** (1972), 94–102. In Russian; translated in *Mech. Solids* **2** (1972).
- [Vigdergauz 2001] S. Vigdergauz, “Genetic algorithm perspective to identify energy optimizing inclusions in an elastic plate”, *Int. J. Solids Struct.* **38**:38 (2001), 6851–6867.
- [Vigdergauz 2006] S. Vigdergauz, “The stress-minimizing hole in an elastic plate under remote shear”, *J. Mech. Mater. Struct.* **1**:2 (2006), 387–406.
- [Vitenberg 1971] Y. P. Vitenberg, Шероховатость поверхности и методы ее оценки, Sudostroenie, Moscow, 1971.

Received 4 Nov 2018. Revised 21 Nov 2018. Accepted 26 Nov 2018.

SHMUEL VIGDERGAUZ: shmuelvigdergauz@gmail.com
 R&D Division, The Israel Electric Corp. Ltd., Haifa, Israel

ISAAC ELISHAKOFF: elishako@fau.edu
 Department of Ocean and Mechanical Engineering, Florida Atlantic University, Boca Raton, FL, United States

JOURNAL OF MECHANICS OF MATERIALS AND STRUCTURES

msp.org/jomms

Founded by Charles R. Steele and Marie-Louise Steele

EDITORIAL BOARD

ADAIR R. AGUIAR	University of São Paulo at São Carlos, Brazil
KATIA BERTOLDI	Harvard University, USA
DAVIDE BIGONI	University of Trento, Italy
MAENGHYO CHO	Seoul National University, Korea
HUILING DUAN	Beijing University
YIBIN FU	Keele University, UK
IWONA JASIUK	University of Illinois at Urbana-Champaign, USA
DENNIS KOCHMANN	ETH Zurich
MITSUTOSHI KURODA	Yamagata University, Japan
CHEE W. LIM	City University of Hong Kong
ZISHUN LIU	Xi'an Jiaotong University, China
THOMAS J. PENCE	Michigan State University, USA
GIANNI ROYER-CARFAGNI	Università degli studi di Parma, Italy
DAVID STEIGMANN	University of California at Berkeley, USA
PAUL STEINMANN	Friedrich-Alexander-Universität Erlangen-Nürnberg, Germany
KENJIRO TERADA	Tohoku University, Japan

ADVISORY BOARD

J. P. CARTER	University of Sydney, Australia
D. H. HODGES	Georgia Institute of Technology, USA
J. HUTCHINSON	Harvard University, USA
D. PAMPLONA	Universidade Católica do Rio de Janeiro, Brazil
M. B. RUBIN	Technion, Haifa, Israel

PRODUCTION production@msp.org

SILVIO LEVY Scientific Editor

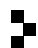
Cover photo: Ev Shafir

See msp.org/jomms for submission guidelines.

JoMMS (ISSN 1559-3959) at Mathematical Sciences Publishers, 798 Evans Hall #6840, c/o University of California, Berkeley, CA 94720-3840, is published in 10 issues a year. The subscription price for 2019 is US \$635/year for the electronic version, and \$795/year (+\$60, if shipping outside the US) for print and electronic. Subscriptions, requests for back issues, and changes of address should be sent to MSP.

JoMMS peer-review and production is managed by EditFlow® from Mathematical Sciences Publishers.

PUBLISHED BY

 **mathematical sciences publishers**
nonprofit scientific publishing

<http://msp.org/>

© 2019 Mathematical Sciences Publishers

Journal of Mechanics of Materials and Structures

Volume 14, No. 1

January 2019

The role of rheology in modelling elastic waves with gas bubbles in granular fluid-saturated media	ADHAM A. ALI and DMITRY V. STRUNIN	1
Some general theorems for local gradient theory of electrothermoelastic dielectrics	OLHA HRYTSYNA and HALYNA MOROZ	25
Effect of surface elasticity on stress intensity factors near mode-III crack tips	XIAN-FANG LI	43
Analytical investigation of free vibrations of a bounded nonlinear bulk-elastic medium in a field of mass forces	EUGENE I. RYZHAK and SVETLANA V. SINYUKHINA	61
A modified shear-lag model for prediction of stress distribution in unidirectional fibrous composites considering interphase	MOHAMMAD HASSAN ZARE and MEHDI MONDALI	97
Nonlinear free vibration of nanobeams based on nonlocal strain gradient theory with the consideration of thickness-dependent size effect	WEI CHEN, LIN WANG and HU-LIANG DAI	119
Energy-maximizing holes in an elastic plate under remote loading	SHMUEL VIGDERGAUZ and ISAAC ELISHAKOFF	139
Anisotropic multimaterial lattices as thermal adapters	MARINA M. TOROPOVA	155
Thermal stress around an elliptic hole weakened by electric current in an infinite thermoelectric plate	KUN SONG, HAO-PENG SONG, PETER SCHIAVONE and CUN-FA GAO	179



1559-3959(2019)14:1;1-X